Cell

Lamellipodial Actin Mechanically Links Myosin Activity with Adhesion-Site Formation

Grégory Giannone,[1,2,6] Benjamin J. Dubin-Thaler,[1,6] Olivier Rossier,[1] Yunfei Cai,[1] Oleg Chaga,[3] Guoying Jiang,[1] William Beaver,[4] Hans-Günther Döbereiner,[1] Yoav Freund,[4] Gary Borisy,[3] and Michael P. Sheetz[1,5,*]
[1] Department of Biological Sciences, Columbia University, New York, NY 10027, USA
[2] CNRS, UMR 5091, Université Bordeaux 2, Bordeaux 33077, France
[3] Department of Cell and Molecular Biology, Northwestern University, Chicago, IL 60611, USA
[4] Department of Computer Science and Engineering, University of California, San Diego, La Jolla, CA 92093, USA
[5] Department of Biological Sciences, PO Box 2408, Columbia University, Sherman Fairchild Center, Room 713, 1212 Amsterdam Avenue, New York, NY 10027, USA
[6] These authors have contributed equally to this work.
*Correspondence: ms2001@columbia.edu
DOI 10.1016/j.cell.2006.12.039

SUMMARY

Cell motility proceeds by cycles of edge protrusion, adhesion, and retraction. Whether these functions are coordinated by biochemical or biomechanical processes is unknown. We find that myosin II pulls the rear of the lamellipodial actin network, causing upward bending, edge retraction, and initiation of new adhesion sites. The network then separates from the edge and condenses over the myosin. Protrusion resumes as lamellipodial actin regenerates from the front and extends rearward until it reaches newly assembled myosin, initiating the next cycle. Upward bending, observed by evanescence and electron microscopy, results in ruffle formation when adhesion strength is low. Correlative fluorescence and electron microscopy shows that the regenerating lamellipodium forms a cohesive, separable layer of actin above the lamellum. Thus, actin polymerization periodically builds a mechanical link, the lamellipodium, connecting myosin motors with the initiation of adhesion sites, suggesting that the major functions driving motility are coordinated by a biomechanical process.

INTRODUCTION

For a cell to migrate, its leading edge must be capable of membrane protrusion, force generation, and adhesion-site formation. While we understand much about these functions individually, how they are spatially and temporally coordinated is largely unknown. An optimal organization of actin filaments, myosin, and adhesion sites is required for fast migration (Gupton and Waterman-Storer, 2006), indicating that actin-filament assembly, force generation, and adhesion are interdependent functions. We seek to understand the molecular mechanisms coordinating these functions, i.e., to find the link between actin polymerization, myosin-force generation, and adhesion-site formation.

The forces driving membrane protrusion are generated by monomeric g-actin polymerizing onto filamentous f-actin at the cell front (Pollard and Borisy, 2003). This system is described as the ''actin treadmill'' because, while actin polymerizes at the front, the entire network flows back and depolymerizes (Ponti et al., 2004; Watanabe and Mitchison, 2002). The balance between polymerization and depolymerization is thought to define a steady-state system that sets the constant width of the actin network observed at the leading edge of migrating cells, the lamellipodium (LP), as well as setting the constant length of a bacteria's actin comet tail (Cameron et al., 2000; Mogilner, 2006; Pantaloni et al., 2001). Recent evidence indicates that the LP overlaps with a less dynamic actin network, the lamellum (LM) (Ponti et al., 2004), and that fast, rearward flowing LP actin has an exploratory function.

While the rearward flow of f-actin in the LP may be in part due to polymerization against the tension of the plasma membrane (Henson et al., 1999; Medeiros et al., 2006; Watanabe and Mitchison, 2002), myosin motors also pull the filaments back (Henson et al., 1999; Medeiros et al., 2006). It appears that polymerization dominates flow at the front of the leading edge, while myosin II (MII) activity causes flow at the back (Henson et al., 1999; Medeiros et al., 2006; Vallotton et al., 2004; Zhang et al., 2003), consistent with MII localization at the back of the leading edge (Verkhovsky et al., 1999).

Myosin activity is also responsible for the organization of proteins into adhesions linking the extracellular matrix (ECM) to the actin cytoskeleton. Force generated by MII on f-actin is responsible for initiation (Galbraith et al., 2002; Rottner et al., 1999b) and maturation of adhesion

Table 1. Protrusion and Retraction Parameters

Condition Measurement		Control	CB	BBI	CalA
Retraction (DIC)	Speed (nm/s)	40 ± 29 (137)		**12 ± 23 (63)*** **	**110. ± 70. (78)*** **
	Duration (s)	4.6 ± 1.9 (125)		**7.0 ± 3.3 (63)*** **	**3.7 ± 1.8 (78)***
Protrusion (DIC)	Speed (nm/s)	42 ± 12 (125)		41 ± 8 (45)	**35 ± 13 (67)***
	Duration (s)	19.2 ± 5.3 (125)		17.8 ± 4.4 (45)	19.2 ± 4 (67)
Period (s) (DIC)		23.8 ± 6.0 (125)	**39.5 ± 15.1 (64)*** **	25.1 ± 5.9 (45)	23.35 ± 5.7 (66)
Meshwork(α-actinin-GFP EPI)	Withdrawal speed (nm/s)	56 ± 28 (88)			
	Growth speed (nm/s)	34 ± 12 (103)	**12 ± 4 (67)*** **		
	Protrusion + growth (nm/s)	76 ± 18 (103)			
	Width after protrusion + growth (nm)	1550 ± 380 (103)			
Protrusion α-actinin transfected cells (EPI)	speed (nm/s)	42 ± 14 (103)			
	duration (s)	21 ± 5 (103)			
Retraction α-actinin transfected cells (DIC)	Speed (nm/s)	47 ± 35 (25)			
	Duration (s)	5.7 ± 1.5 (25)			
Period (s) transfected cells (DIC)	GFP	24 ± 4 (30)			
	α-actinin-GFP	26 ± 5 (109)			
	VASP-GFP	24 ± 4 (54)			
	MLC-GFP	25 ± 4 (49)			

Statistically different values are in bold. Bonferroni, ***P < 0.001; **P < 0.01; *P < 0.05. t-test, ***P < 0.001, **P < 0.05.

sites (Schoenwaelder and Burridge, 1999). Adhesion-site formation has been observed back from the leading edge, at the LP-LM junction (Ponti et al., 2004; Rottner et al., 1999a; Zaidel-Bar et al., 2003), which may result from forces generated by the LM. However, integrins near the front of the cell (<0.5 μm from edge) have a higher affinity for the ECM, form more stable integrin-cytoskeleton links, and undergo force-dependent reinforcement compared to integrins further back (Jiang et al., 2006; Nishizaka et al., 2000). In addition, early adhesion-site formation has the same periodicity as myosin-dependent edge retractions (Giannone et al., 2004), suggesting a mechanical relationship between edge retractions and early adhesion-site formation.

Recent studies have provided evidence for non steady-state dynamics in the LP (Dubin-Thaler et al., 2004; Giannone et al., 2004; Ponti et al., 2004). Both oscillating rates of actin polymerization and depolymerization (Ponti et al., 2004) combined with the discovery of periodic contractions of the leading edge (Giannone et al., 2004) are inconsistent with a steady-state model. Because both oscillations in polymerization rate and edge protrusion occur on the same timescale and in the same location, LP actin dynamics and edge retraction could be related, although the mechanism is unknown.

We previously found that protrusion, adhesion-site formation, and force generation occurred with a remarkably stable period at the leading edge (Giannone et al., 2004). For sake of clarity, we will refer to this region as the LP contractile module. Using the molecular clocking in the LP contractile module, we could decipher how the architecture and dynamics of actin networks are coupled to force generation and adhesion-site initiation. We defined a cohesive but labile actin network, LP actin, which undergoes periodic separation from the cell edge, condensation, and regeneration. Myosin at the back of the LP contractile module pulls on the regenerated LP actin network, which causes upward bending, edge retraction, adhesion-site initiation at the cell front, and finally, separation of the actin network. Therefore, the LP actin operates like a cyclic mechanical bridge, synchronizing MII force generation with adhesion-site initiation and clocking the cycles of edge protrusion. These findings show that mechanical signaling is as crucial as biochemical signaling during cell migration.

RESULTS

Actin Waves Do Not Initiate Periodic Contractions

The leading edges of migrating and spreading cells exhibit periodic contractions on fibronectin (FN) (Giannone et al., 2004). Differential interference contrast (DIC) microscopy revealed that periodic contractions coupled with the rearward movement of waves of matter from the edge. Total

MIIB Control	MIIB −/−	Stiff Gels	Interm. Gels	Low [FN]	High [FN]
53 ± 57 (46)	**17 ± 16 (80)*** **	41 ± 33 (115)	**15 ± 20. (131)*** **	38 ± 27 (43)	44 ± 39 (29)
6.6 ± 3.1 (46)	7.7 ± 3.4 (80)	**5.6 ± 2.0 (115)** **	**8.1 ± 2.7 (131)*** **	**6.7 ± 3.1 (43)*** **	5.6 ± 1.8 (27)
35 ± 10 (46)	**29 ± 12 (65)** **	**37 ± 11 (103)***	46 ± 14 (73)	27 ± 10 (55)	35 ± 14 (28)
21.7 ± 7.0 (46)	**17.0 ± 6.3 (64)*** **	17.4 ± 4.7 (103)	19.2 ± 4.9 (73)	**16.2 ± 7.6 (55)** **	17.8 ± 3.5 (28)
28.3 ± 7.7 (46)	24.7 ± 8.5 (64)	22.9 ± 5.2 (103)	26.4 ± 2.7 (73)	23.6 ± 10.6 (43)	23.4 ± 4.4 (27)

internal reflection fluorescence (TIRF) microscopy showed similar waves of α-actinin-GFP and MLCK-GFP, molecules that are, along with arp2/3 and ADF/cofilin (Ponti et al., 2004), characteristic actin binding proteins (ABPs) in the LP. The period between edge retractions (23.8 ± 6.0 s, Table 1) and the period for DIC and ABP waves to travel across the LP width were identical. Because MII localizes at the back of the leading edge (Verkhovsky et al., 1999), the most obvious candidate for initiating contraction was a contractile signal associated with actin in the DIC waves. To test the causal relationship between DIC waves and edge retraction, we stopped and restarted the periodic contractions to watch the initial steps of the cycle. Low concentrations of jasplakinolide (200 nM) transiently disrupted cell-edge protrusion effectively "resetting" the protrusion/contraction cycle (Figure 1A). Restart of actin polymerization and cell-edge protrusion was immediately associated with the generation of periodic contractions. Remarkably, the first contraction was initiated before the first DIC wave, demonstrating that contraction can initiate without DIC waves or any material carried with the waves.

Periodic Contraction Correlates with Regeneration of Lamellipodial Actin

If the waves were not starting the next contraction, what could be the periodic phenomenon initiating the next contraction? Using epifluorescence (EPI) microscopy with α-actinin-GFP as a reporter for LP actin, we observed gaps in α-actinin-GFP fluorescence corresponding to periodic LP actin formation and subsequent separation from the cell edge (Figure 1B). LP actin grew rearward from the edge at a speed of 34 ± 12 nm/s relative to the substrate during both edge protrusion (lasting 19.2 ± 5.3 s) and retraction (lasting 4.6 ± 1.9 s) (Figure 1C and Table 1). At the transition from edge retraction to protrusion, the newly grown LP actin separated from the edge at a speed of 56 ± 28 nm/s relative to the substrate, forming the rearward moving ABP wave (Figures 1B and 1C and Table 1). The separation was immediately followed by regeneration of α-actinin-GFP from the now protruding edge. Therefore, LP actin periodically regenerated and separated in phase with protrusion and retraction. LP actin regenerated at a speed of 76 ± 18 nm/s (edge protrusion plus rearward network growth), reaching the back of the LP contractile module, 1550 ± 380 nm from the edge, at the moment the next contraction began (Table 1). Therefore, the growing LP actin network appeared to trigger the contraction. The speed of edge protrusion and period between contractions in α-actinin-GFP transfected cells was identical to nontransfected cells (see Table 1). This regenerative process was not occurring in cells spreading without periodic contractions on poly-L-lysine (PLL) (Figure S1A), indicating that integrin-mediated adhesion is involved.

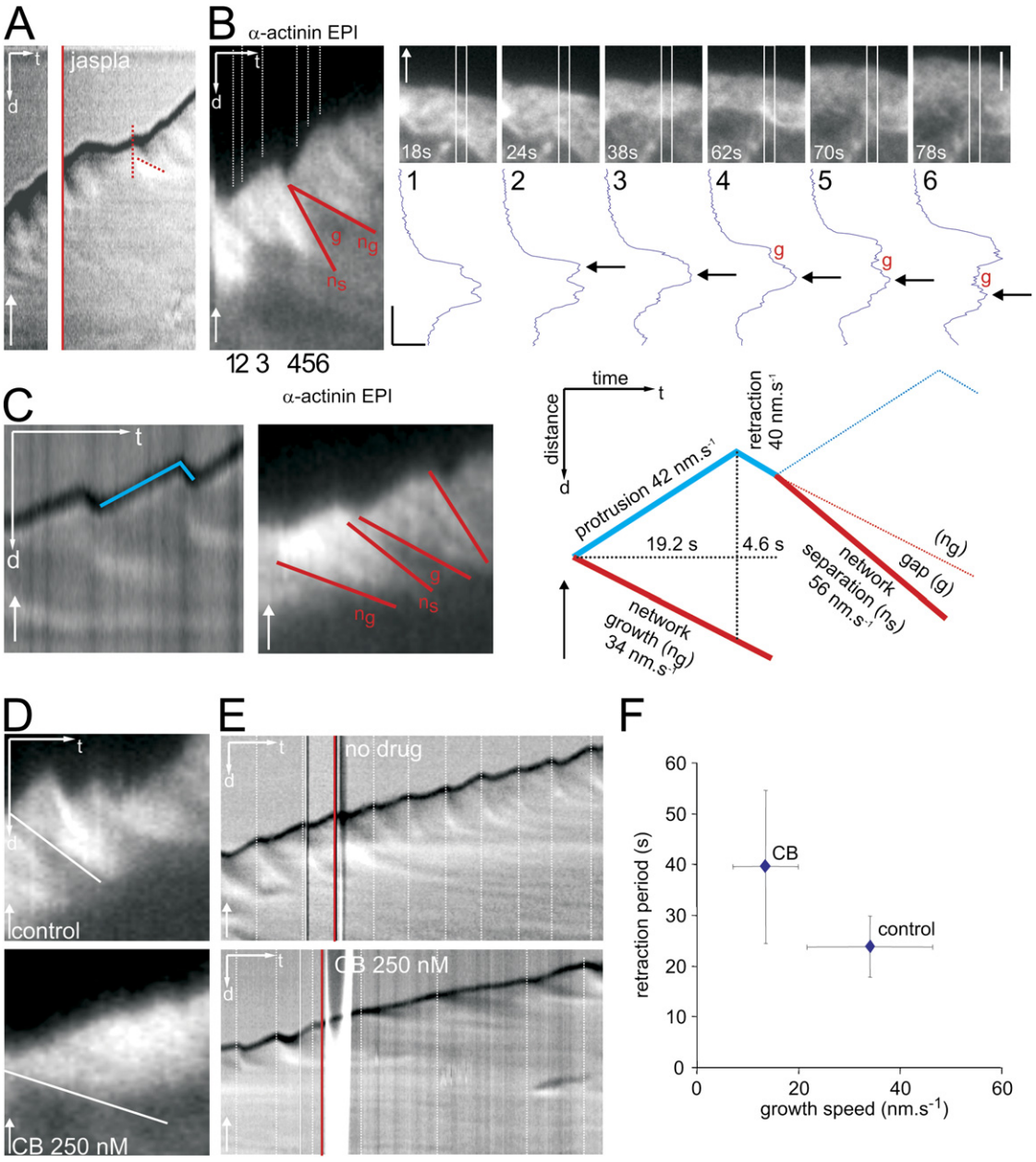

Figure 1. The Period of Retraction Depends on Lamellipodial-Actin Growth and Regeneration during the Contractile Cycle

(A) DIC kymograph of a MEF spreading on FN (10 μg/ml) showing the generation of periodic waves during periodic contractions. Perfusion of jasplakinolide (200 nM, red line) induces transient cessation of periodic contractions. The cycle resumes by an edge retraction followed by a DIC wave (dashed red lines). Time bar, 30 s (t); scale bar, 1 μm (d).

(B) α-actinin EPI (left) kymograph. Note the periodic network growth (n_g) and separation (n_s) of α-actinin from the cell tip that created gaps (g) in the α-actinin fluorescence (Movie S1). The dotted lines correspond to the time where pictures 1–6 (right top) were acquired. Rectangles in pictures 1–6 depict the region used to generate the kymograph and intensity profiles (right bottom). The intensity profiles show growth, separation (black arrows), and gap formation ("g") in α-actinin network. Left, t = 30 s; d = 1 μm. Right top, scale bar 1 μm. Right bottom, intensity bar (horizontal) arbitrary unit; scale bar, (vertical) 1 μm.

(C) DIC (left) and α-actinin EPI (middle) kymographs with lines marking the displacement of the cell edge (blue) and the α-actinin network growth (n_g), separation (n_s), and gap formation (g) (red). The schematic kymograph (right) shows the parameters we quantified that are summarized in Table1.

(D) α-actinin EPI kymograph before (up) and after (bottom) perfusion of CB (250 nM). The rate of LP-actin growth (slope of white line) is reduced by CB treatment (Movie S2). t = 30 s; d = 2 μm.

(E) DIC kymograph. Perfusion of a control solution (up) does not change periodic contractions or DIC waves. Perfusion with 250 nM CB solution (bottom) decreases the period of retraction (Movie S3). t = 30 s; d = 2 μm.

(F) Relationship between the retraction period and the actin-network growth speed. Error bars show standard deviation. White arrows indicate direction of protrusion.

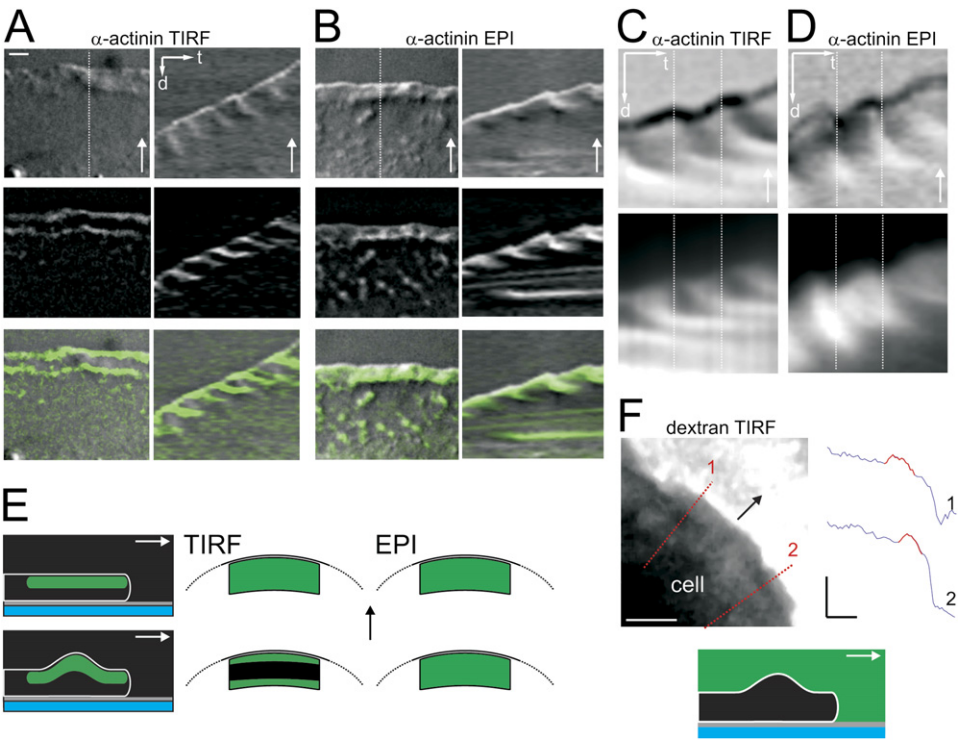

Figure 2. Lamellipodial-Actin Bending

(A) Micrographs (left) and kymographs (right) of DIC (top), α-actinin TIRF (middle), and merge (bottom). The dashed line depicts the region used to generate the kymographs (Movie S4). Left, scale bar, 2 μm. Right, t = 30 s; d = 2 μm.

(B) Identical to (A) except with α-actinin EPI (middle) (Movie S5).

(C) Kymographs of DIC (top) and α-actinin TIRF (bottom). Dashed lines mark the start of edge retraction. Note that LP-actin bending, visualized in TIRF by the loss in α-actinin-GFP fluorescence, initiates simultaneously with the start of edge retraction. t = 30 s; d = 2 μm.

(D) Kymographs of DIC (top) and α-actinin EPI (bottom). Dashed lines mark the end of edge retraction. Note that the gap between LP actin and the edge, visualized by EPI, occurs 5 s after the start of edge retraction simultaneously with the end of the retraction. t = 30 s; d = 2 μm.

(E) Schematic of the α-actinin network before (top) and after (bottom) edge retraction showing a side view (first column), imaging by TIRF (second column), and EPI (third column). Green represents α-actinin fluorescence, white outlines the LP contractile module, gray corresponds to FN, and the blue rectangle corresponds to the glass coverslip.

(F) MEF generating periodic contractions in a medium containing high molecular weight fluorescein dextran imaged with TIRF (top left). Fluorescence intensity profiles (top right) taken along dashed lines 1 and 2 show that the height of the LP contractile module peaks (red line) at a position corresponding to DIC waves. A schematic representation of the bending LP contractile module is shown (bottom). Colors correspond to (C), except green represents fluorescein. Top left, scale bar, 2 μm. Top right, intensity bar (vertical), arbitrary unit; scale bar (horizontal), 1 μm.

Contractile Cycle Period Set by LP-Actin Growth Rate

We next tested if contraction was initiated by the growing LP actin. Cytochalasin B (CB), an inhibitor of actin polymerization (Sampath and Pollard, 1991), was used to decrease the LP-actin growth rate. Following treatment with 250 nM of CB, EPI revealed that LP-actin growth decreased from 34 ± 12 nm/s to 12 ± 4 nm/s (Figures 1D and 1F and Table 1). The CB-treated cells still generated periodic contractions, but the period increased from 23.8 ± 6.0 to 39.5 ± 15.1 s (Figures 1E and 1F and Table 1). These experiments established an inverse relationship between LP-actin growth rate and the period between contractions (Figure 1F). This evidence, along with the knowledge that DIC waves alone do not initiate contractions, suggests that growing LP actin alone can trigger contractions.

Periodic Contractions Bend the Lamellipodium

Using parallel DIC and TIRF microscopy, we were surprised to find that waves of α-actinin-GFP in TIRF did not continually overlap with the DIC waves (Figure 2A). TIRF fluorescence was lost simultaneously with the start of edge retraction (Figure 2C). EPI microscopy, however, revealed continual colocalization between DIC and α-actinin-GFP waves, even during edge retraction (Figures 2B and 2D). Those results suggested that LP actin lifted above the shallow TIRF-excitation field. Rhodamine-phalloidin (Figures S1C and S1D) and MLCK-GFP (Figure 3F) also exhibited fluorescence loss in TIRF during edge retraction. This evidence indicates that the LP actin bends upward during edge retraction (Figure 2E, schematic).

To further confirm LP-actin bending, we added high molecular weight fluorescent dextran (2,000,000 kDa) to the

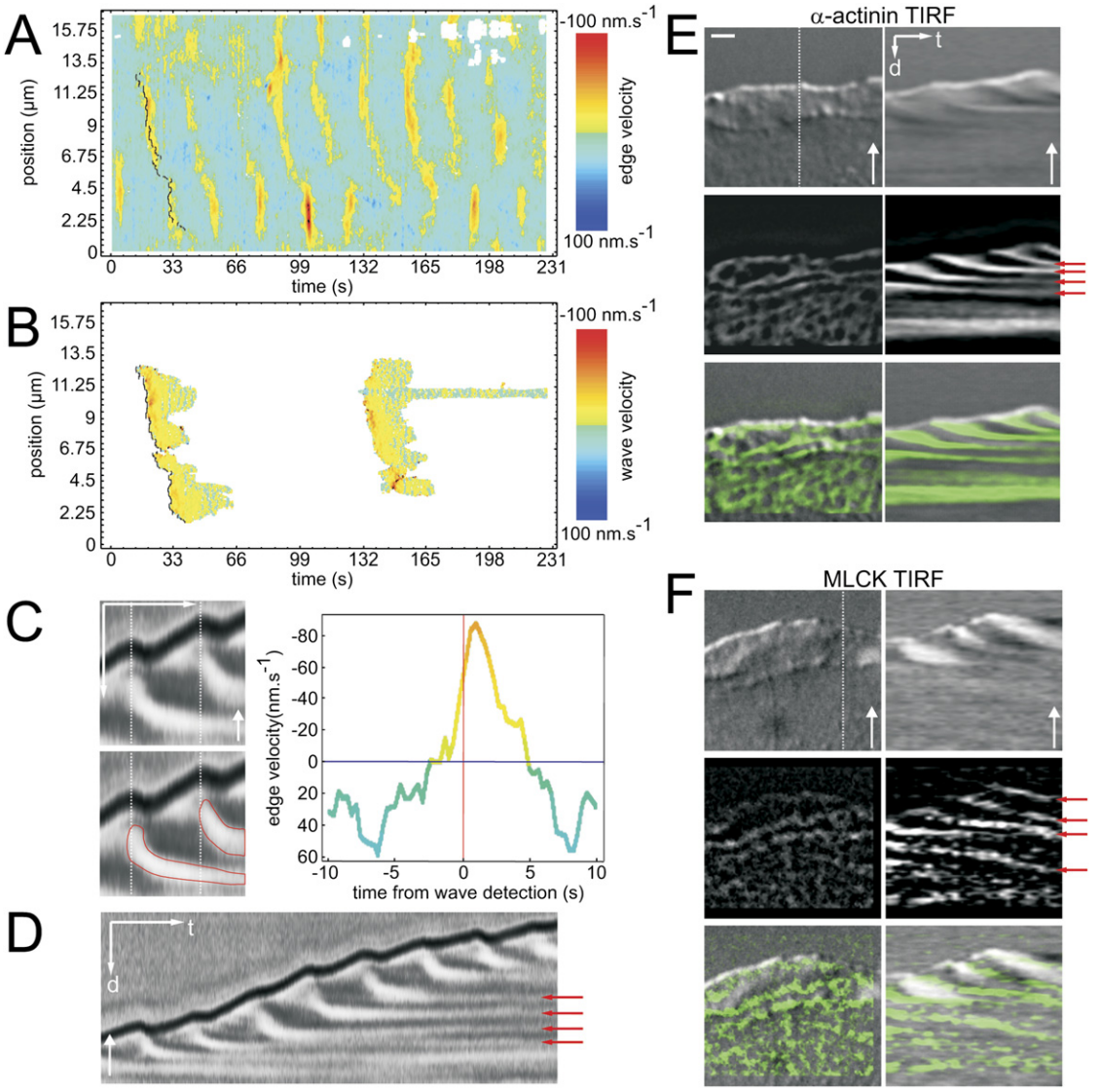

Figure 3. Mechanical Connections between Cell Edge and the Lamellipodial Actin Are Broken Inducing Separation and Condensation of Lamellipodial Actin

(A) Cell-edge velocity plotted as a function of time and position along the edge of a spreading MEF (Movie S6). The cell edge was detected using computer vision from which edge velocity was calculated (see Experimental Procedures). Lateral propagation of retraction is visible as diagonal yellow lines.

(B) Velocity of the rearward movement of two DIC waves plotted as a function of time and position along the cell edge. Note that the front of the waves correspond to edge retractions in (A). For sake of clarity, two of seven detected waves are shown.

(C) DIC kymograph from the cell in Figure 3A shows that DIC wave initiates simultaneously with the start of edge retraction (left). In the bottom kymograph the white part of the DIC wave is outlined in red. Dashed lines mark the start of edge retraction. Time bar, 30 s; scale bar, 2 μm. Shown is a plot of cell-edge velocity during retraction as a function of time relative to the initial detection of the DIC wave peak (red line) (right). The analysis reveals that the DIC wave peak is detected shortly (1.5 ± 1.5 s, 803 kymographs, seven waves) after the start of the edge retraction.

(D) DIC kymograph from the cell in Figure 3A shows the generation of DIC waves and their condensation into persistent structures (red arrows). t = 30 s; d = 2 μm.

(E) DIC (top), α-actinin-GFP TIRF (middle), and merge (bottom) micrographs (left column) and kymographs (right column). Dotted lines depict the regions used to generate the kymographs. Note the condensation of α-actinin into bundles (red arrows) (Movie S7). Left, scale bar, 2 μm. Right, t = 30 s and d = 2 μm.

(F) Identical to (E), except fluorescence is GFP-MLCK. White arrows indicate direction of protrusion.

extracellular medium. TIRF imaging revealed lines of decreased dextran fluorescence parallel to the edge in the LP-actin region, indicating that the dorsal surface of the LP contractile module moved upward (Figure 2F). We then performed TIRF experiments on cells expressing cytosolic GFP to detect lifting of the ventral plasma membrane. In this case, we observed no fluorescence loss (Figure S1B). These experiments, combined with the observation of adhesion sites in the regions of LP bending (Figures 5D and Figure S1E), indicated that forces in the LP-contractile module caused LP actin to bend upwards, above areas with physical links to the surface. Therefore, inward, vertical forces were exerted on the LP actin during edge retraction.

Regeneration of LP Actin Followed Its Mechanical Separation and Condensation into Lamellar Bundles

We hypothesized that inward pulling forces, exerted on the LP actin from the beginning of edge retraction, caused simultaneous edge retraction and bending until the LP-actin network mechanically separated from the edge. To determine if there was a mechanical link between LP actin and the cell edge, we compared the dynamics of DIC waves (Figure 3B) and edge retraction (Figure 3A). We used DIC waves as an indicator for retracting LP-actin dynamics since they colocalized (Figures 2B and 2D). A computer vision algorithm was trained to simultaneously detect the cell edge and the DIC-wave peak (Figure S2). The analysis revealed that the DIC-wave peak initiated shortly (1.5 ± 1.5 s) after the start of edge retraction (Figure 3C), suggesting that the two structures are mechanically linked. In addition, the speed of the DIC-wave rearward movement correlated with the speed of edge movement only during retraction (Pearson *r* of 0.33), suggesting that stronger pulling forces exerted on the LP-actin network resulted in a faster retraction speed.

If LP actin was mechanically attached to the cell edge while being pulled back, the edge could not protrude until this attachment was disrupted. We observed exactly that: resumption of cell-edge protrusion directly following separation of α-actinin-GFP fluorescence from the edge (Figures 1B, 1C, 2B, 2D, S3D, and S3E). In addition, we observed laterally propagating retractions (310 ± 190 nm/s, n = 10 events) (Figures 3A, S3A, and S3B) that corresponded with lateral propagation of LP-actin separation and resumption of cell-edge protrusion, as visualized by DIC and EPI microscopy of α-actinin-GFP (Figure S3C). To check if the LP actin was detaching from the polymerization machinery at the edge, we used parallel DIC and TIRF microscopy to observe VASP, a protein that localizes to the cell-edge and adhesion sites and regulates actin polymerization (Bear et al., 2002; Fradelizi et al., 2001; Rottner et al., 1999a). After edge retraction, VASP-GFP split between the edge and initiating adhesion sites (Figure S3F), suggesting that the separation was occurring within the polymerization machinery. However, VASP-GFP did not move with the DIC wave.

If LP actin detached from the edge, additional material should be concentrated at the back of the LP contractile module. Close analysis of the DIC sequences showed that waves condensed into linear bundles parallel to the edge and persisted in the LM even after generation of subsequent waves (Figure 3D). In TIRF experiments, these dense DIC structures colocalized with actin bundles resulting from condensation of rearward-moving LP actin and contained α-actinin-GFP and MLCK-GFP (Figures 3E and 3F). These observations indicated that the inward forces pulling on the LP actin were able to separate the actin network from the edge as well as condense and reorganize the LP actin into dense actin bundles at the back of the LP contractile module.

Separation of LP Actin Network from the Edge Depends on MII Activity

Inhibition of the MII activator, MLCK, reduces the number of cells generating periodic contractions (Giannone et al., 2004). To test if MII was pulling and detaching LP actin, we modulated MII activity. Blebbistatin (BBI) selectively inhibits MIIA and MIIB activity (Straight et al., 2003), and Calyculin A (CalA) increases MII activity (Vallotton et al., 2004). BBI decreased the speed of edge retraction and increased retraction duration (Figures 4A and 4B and Table 1), while CalA increased the speed of edge retraction and decreased retraction duration (Figures 4A and 4B and Table 1). BBI or CalA did not affect the duration of edge protrusion. The direct dependence of retraction speed on MII activity along with the inverse dependence on retraction duration (Figure 4B) indicated that MII activity generated forces that induced edge retraction and LP-actin separation. Increasing and decreasing the FN concentration did not greatly alter retraction parameters (Table 1). However, decreasing FN concentration reduced the number of cells (less than 5% of cells) exhibiting periodic contractions, while ruffling increased. Decreasing substrate stiffness decreased the retraction speed and increased its duration (Table 1), suggesting that integrin-mediated adhesions were sustaining MII force generation. Interestingly, on soft substrates, early adhesion sites were moving reward (6 ± 3 nm/s, n = 19 events); but on glass, adhesion sites were not moving detectably.

To complement the chemical inhibitor studies, we manipulated MII gene expression. In MIIB knockout (KO) fibroblasts, edge-retraction speed decreased compared to control, and in 60% of cells, the LP contractile module deadhered and ruffled (Figures 4C and 4D and Table1). Furthermore, in MIIB KO cells in which we knocked down MIIA via siRNA (Cai et al., 2006), 60% of the population displayed no visible periodic contractions compared to 4% in MIIB KO cells (Figures 4C and 4D). Therefore, MII activity appeared essential in the generation of periodic contractions.

We next examined MII distribution using myosin light chain-EGFP (MLC-EGFP) (Tamada et al., 2007) (Figure 5A). Simultaneous TIRF and DIC microscopy revealed that MLC-EGFP aggregates formed preferentially at the back of the LP contractile module. MLC-EGFP aggregates assembled following edge retraction at the same location

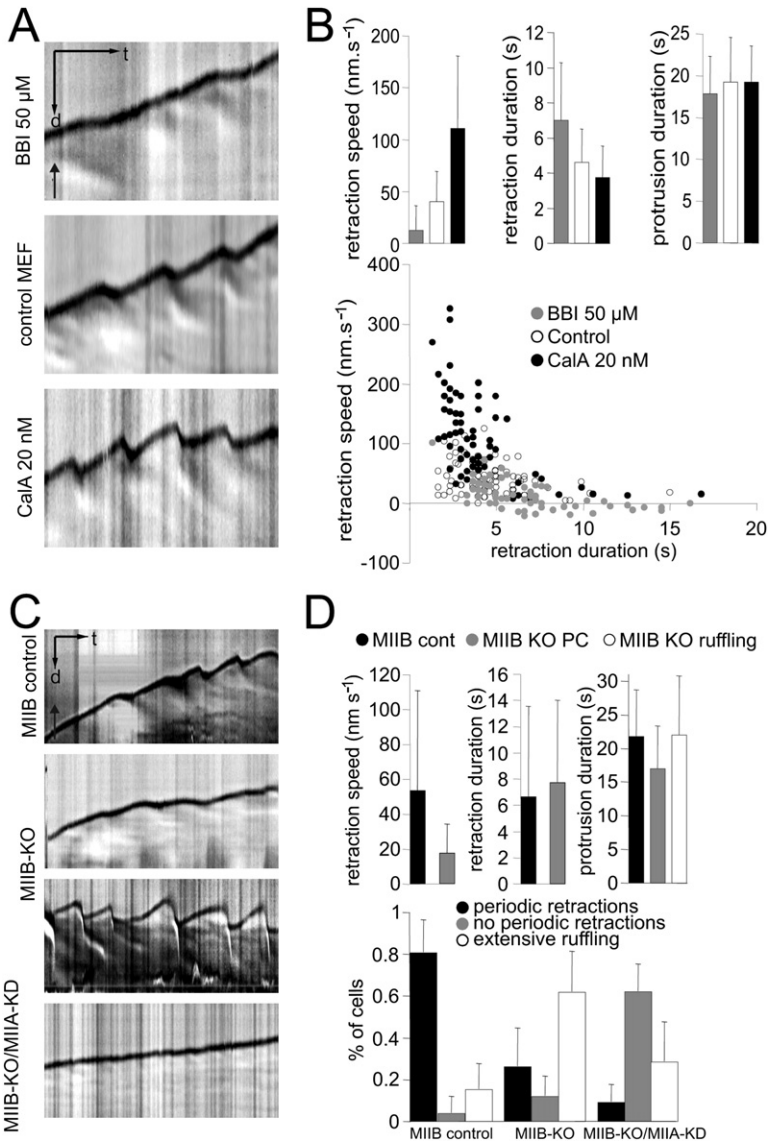

Figure 4. Edge Retraction Depends on MII Activities

(A) DIC kymographs shows that retraction speed is decreased with BBI (50 μM) (top) when compared to controls (middle), while CalA (20 nM) increases retraction speed (bottom) (Movie S8). t = 30 s; d = 2 μm.

(B) Bar graphs of periodic contractions retraction speed (left) and duration (middle) and protrusion duration (right) for cells treated with BBI (gray), control (white), and CalA (black). Scatter plot shows an inverse relationship between retraction speed and retraction duration (bottom). Error bars show SD.

(C) DIC kymographs show that a MIIB control cell (top) generates stronger retractions compared to a MIIB-KO cell (middle top). MIIB-KO also ruffle extensively (middle bottom) (Movie S9), while a MIIB-KO/MIIA-KD cell generates no periodic contractions (bottom) (Movie S10). t = 30 s; d = 2 μm.

(D) Bar graphs show retraction speed (top left) and duration (top middle) and protrusion duration (top right) for MIIB control cells (black) and MIIB-KO cells (gray) during periodic contractions, while MIIB-KO cells generating extensive ruffling show comparable protrusion speed (white). Bar graphs represent the percentage of cells displaying periodic contractions (black), no periodic contractions (gray), and extensive ruffling (white), for MIIB control cells (bottom left), MIIB-KO cells (bottom middle), and MIIB-KO/MIIA-KD cells (bottom right). Error bars show SD. Black arrows indicate direction of protrusion.

and time as actin-bundle formation (Figure 5A). Interestingly, on FN the rearward movements of MLC-EGFP aggregates were slow (10 ± 4 nm/s, n = 39 events) and linked in a network (Figure S4B). Conversely, on PLL MLC-EGFP rearward movements were fast (63 ± 11 nm/s, n = 35 events) and unstructured (Figure S4A), suggesting that integrin-mediated adhesions were involved in the organization of MII.

LP-Actin Pulling Initiates Adhesion-Site Formation

Integrin and paxillin form rows during periodic contractions (Giannone et al., 2004). We performed simultaneous TIRF and DIC microscopy with paxillin-GFP or VASP-GFP to test if contractions initiated adhesion sites (Figures 5B and S3F). Adhesion sites initiated during edge retraction 390 ± 210 nm (n = 23 events) back from the edge (Figure 5B). The proximity of adhesion-site initiation to the region where edge retraction and LP-actin separation occurred suggested that MII pulling on LP actin could result in force-dependent adhesion formation. To test if forces were exerted on integrins at the cell edge during retraction, we performed laser-trap experiments. Using beads coated with dilute FN, we decreased the probability of integrin coupling to the actin cytoskeleton (Jiang et al., 2003). In those conditions, initiation of the coupling with the actin cytoskeleton was triggered preferentially during cell-edge retraction, 1.7 ± 1.7 s (n = 9 events) after initiation of contraction (Figure 5C). In addition, VASP split between the cell edge and initiating adhesion sites (Figure S3F), suggesting that a complex containing at least integrins and VASP was released from the edge to initiate adhesion sites. These results showed that LP actin transmitted MII generated forces to integrins at the cell front, initiating adhesion sites.

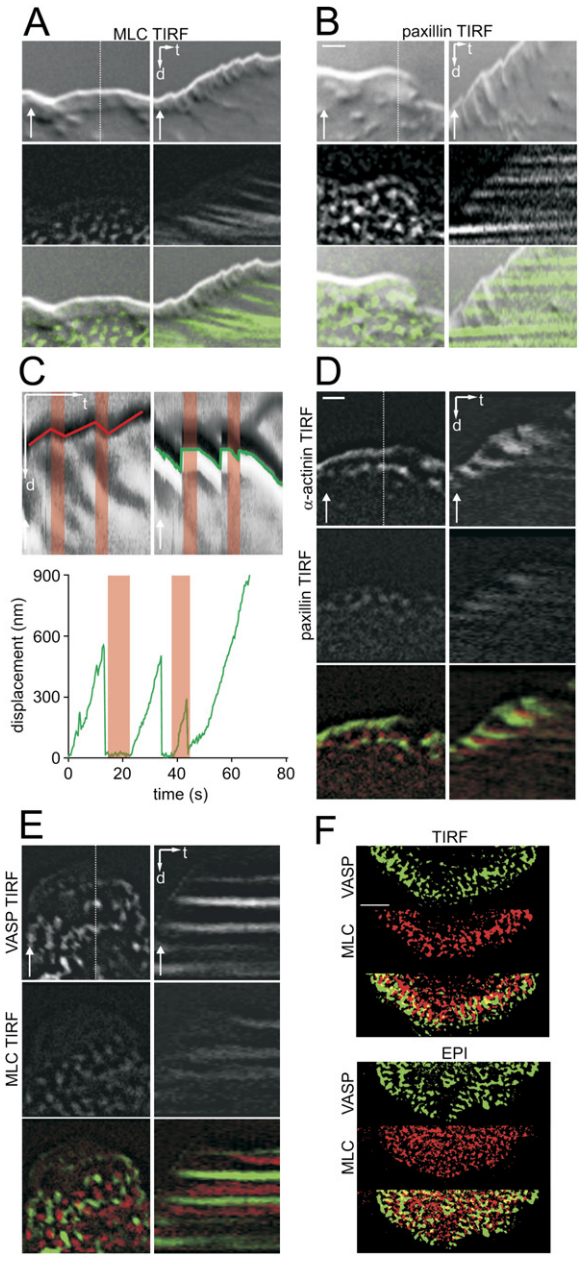

Figure 5. Periodic Contractions Initiate Adhesion-Site Formation

(A) DIC (top), MLC-EGFP TIRF (middle), and merge (bottom) micrographs (left column) and kymographs (right column). Note that MLC clustered at the back of the LP contractile module (Movie S11).

(B) Same as (A) except with paxillin-GFP TIRF. Note that adhesion sites initiated close to the cell edge, between the cell tip and the previous DIC wave (Movie S12).

(C) Laser-trap experiment using beads coated with diluted FN7-10 trimers. Beads were positioned on the tip of the protruding cell edge using a laser trap during the generation of periodic contractions. DIC kymographs depict the movement of the cell edge (upper left, red line) and the movement of an FN-coated bead (upper right, green line). Displacement versus time plot (bottom) show that the bead is periodically connecting to the actin flow during the retraction (red strips), being moved rearward until the force applied by the laser trap break its connection with actin, pulling back the bead in the trap center (Movie S13).

(D) α-actinin-GFP TIRF (top), paxillin-DsRed TIRF (middle), and merge (bottom) micrographs (left column) and kymographs (right column). Note that adhesion sites were present in the area where the LP actin was bending up. Note that α-actinin condenses behind adhesion sites initiated by the previous retraction (Movie S14).

(E) Same as (D) but with VASP-GFP TIRF (top), MLC-mRFP TIRF (middle), and merge (bottom). Note the succession of adhesion site rows and MLC aggregates (Movie S15).

(F) Thresholding of VASP-GFP (green) and MLC-mRFP (red) fluorescence was performed to quantify the colocalization (yellow) of protein clusters, both in TIRF (up) and in EPI (bottom). MLC and VASP clusters were excluded (Movie S16). t = 30 s; d = 2 μm. White arrows indicates protrusion direction. Dashed lines indicate the region used to generate kymographs.

Pulling on LP actin would require an anchor against which an opposite force could be applied. We tested if previous adhesion sites might provide this anchoring structure. TIRF microscopy experiments using α-actinin-GFP and paxillin-DsRed demonstrated that the LP-actin network bundled behind the adhesion sites that had formed during the previous contraction (Figures 5D and S1E). We tested if MII aggregates formed behind these adhesion sites. VASP-GFP and MLC-mRFP revealed a succession of adhesion-site rows followed by MLC aggregates (Figures 5E and 5F). The same results were obtained for both EPI and TIRF as well as with paxillin as an indicator of adhesions (Figure S4C). Moreover, quantification of the colocalization in time-lapse showed only 4% ± 1% (108 frames, 4 cells) of overlap between MLC-mRFP and VASP-GFP even in regions with 51% ± 6% coverage by clusters (Figure 5F), demonstrating that MLC was excluded from adhesion sites. Despite the dynamics of MLC and adhesion sites, the movement of MLC was channelled around adhesion sites (Figure S4B). Together, these results indicate that there are physical interactions between MLC and adhesion sites that lead to their physical separation.

Electron Micrographs Reveal a Dense and Cohesive Network of Lamellipodial Actin

To extend the light microscope results, we performed correlative light/electron microscopy (Svitkina and Borisy, 1998) on cells transfected with α-actinin-GFP. To ensure LP actin was not disrupted by sample preparation, we followed the periodic contractions in time-lapse EPI and DIC microscopy during EM sample preparation. The fluorescence pattern (Figure 6A) and DIC waves (Figures 6B and 6C) were identical before and after preparation, indicating that the LP-actin network was preserved. Comparing EM to α-actinin-GFP fluorescence (Figures 6D, 6E, and 6G) revealed that LP actin corresponded to a cohesive, dense actin network (Figures 6F, top, and 6G, right). Lamellar regions with less α-actinin-GFP fluorescence showed a sparsely organized actin network (Figures 6F, bottom, and 6G, right). The growing LP actin was visible at the front of the LP contractile module (Figure 6G,

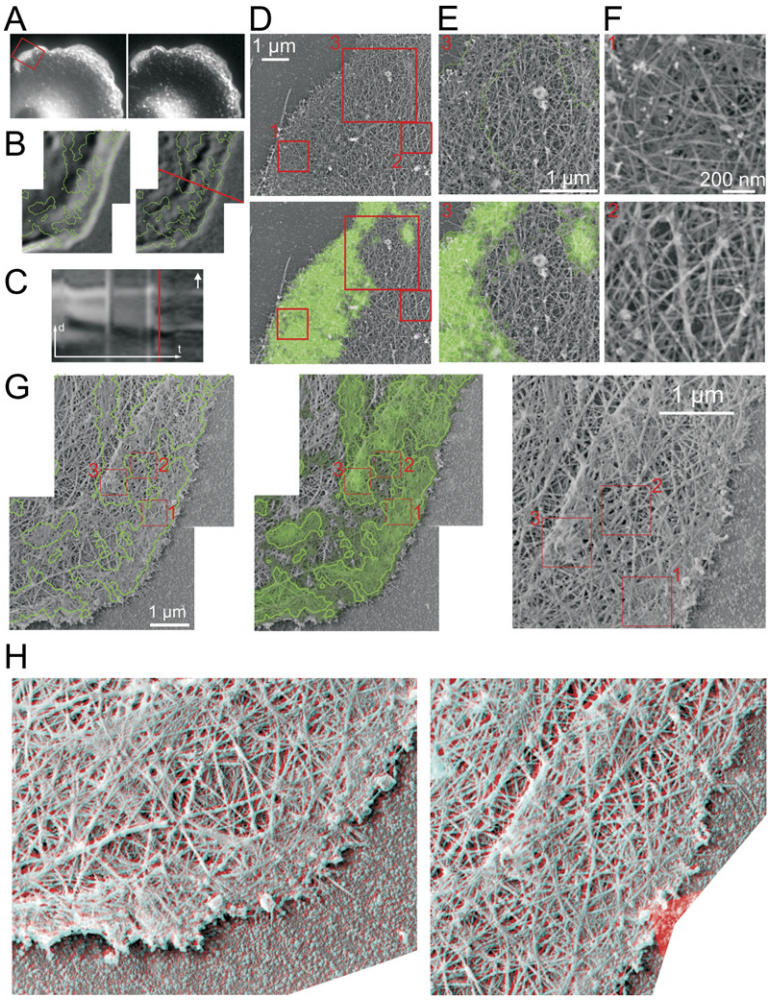

Figure 6. Lamellipodial Actin Is a Dense and Cohesive Network above the LM

(A) Spreading MEF generating periodic contractions. LP actin seen by α-actinin-GFP (left) is preserved after extraction/fixation (right) for EM visualization.

(B) DIC image of spreading MEF generating periodic contractions just before (left) and just after (right) extraction. The green contours denote high α-actinin-GFP fluorescence.

(C) DIC kymograph generated from the region depicted by the red line in (B). Vertical line indicates detergent extraction. The DIC wave is unchanged by extraction.

(D) Blowup of the subregion in (A) seen in EM (top) and merged with α-actinin fluorescence (green, bottom).

(E and F) Higher-resolution blowups of the regions depicted in (D) showing that the α-actinin-GFP fluorescence colocalizes with a dense ultrastructure. Green contour in (E) denotes high α-actinin-GFP fluorescence.

(G) Visualization of the cytoskeletal ultrastructure (cell from B and C) by EM merged with α-actinin fluorescence contours (left) and with α-actinin fluorescence (middle) showing colocalization of α-actinin with the dense actin network visible in detail (right) (stack, Movie S17). Note the LP-actin growth (1), gap in the LP actin (2), and LP-actin bundle (3).

(H) Stereo anaglyphs (subregions from G, left panel) showing the dense structure corresponding to LP actin atop a more sparse structure (left and right) and LP-actin bending during contraction (left). Stereo glasses should be worn with blue filter over the right eye.

box 1). Like α-actinin-GFP fluorescence, this growing LP-actin network was discontinuous and revealed an underlying actin network (Figure 6G, box 2). Further back from these gaps, condensed LP actin corresponded to the ABP wave (Figure 6G, box 3). Note that the DIC wave (Figures 6B and 6C), α-actinin-GFP fluorescence (Figure 6G), and the dense and cohesive network visible in EM (Figure 6G) were colocalized (see stacks, Movie S17). LP actin formed a network distinct from other filaments, suggesting that these other filaments may be part of the LM. Stereo views of the LP contractile module revealed that the detached LP actin was indeed located above the LM (Figure 6H). This three-dimensional perspective also confirmed bending of both networks (Figure 6H, left). These results indicated that LP actin formed a separate, cohesive network atop the sparser network of the LM.

DISCUSSION

Our results detail a novel, biomechanical view of the leading edge of migrating and spreading cells. In that view, LP actin forms a labile mechanical link between the actin-polymerization complex at the edge and the myosin motor activity at the back. The LP contractile module has two actin layers, with LP actin being above the LM actin and the LM actin resisting compression. This physical configuration allows MII force, actin polymerization, and adhesion formation to be mechanically coordinated. Although biochemical changes are important, crucial elements are mechanical in nature.

Initiation of Adhesion Sites during Periodic Contractions

With each contraction, integrins are concentrated into substrate adhesions containing VASP and paxillin (Figure 5). In addition, we find that FN-coated beads held in a laser trap at the edge attach to the cytoskeleton preferentially when contractions occur (Figure 5C). Particularly interesting is the observation that VASP is split between the edge and initiating adhesion sites (Figure S3F). This suggests that components involved in attachment of integrins to the cytoskeleton and actin polymerization are activated and released at the cell edge as the contractions occur. These results extend previous observations of

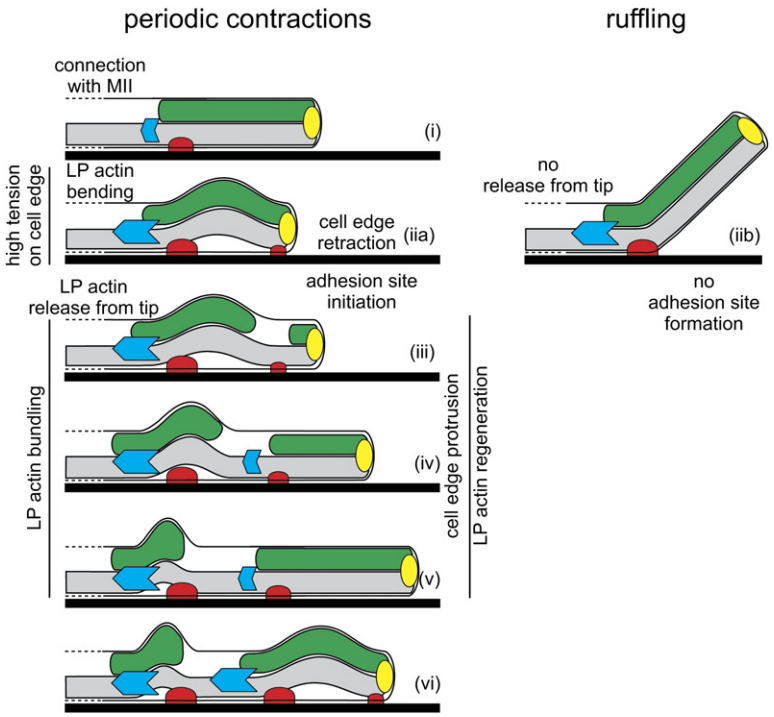

Figure 7. Schematic Representation of Lamellipodial-Actin Periodic Regeneration

The LP actin (green) is above the LM (gray). Polymerization at the front of the LP-actin network causes the back of the network to grow toward the back of the LP contractile module until it reaches an adhesion site (i) where a MII cluster (blue) forms. MII pulls the LP actin, generating high tension on the cell front, causing LP bending, edge retraction, and initiation of new adhesion sites (red) on the ECM (black rectangle) (iia). The LP actin continues to be pulled until it is released from the tip (iii) and edge protrusion restarts. A new LP actin network immediately resumes growth, suggesting that the actin polymerization machinery (yellow) is still present at the cell tip (iv). The released LP actin, still pulled by MII, further condenses into a bundle at the back of the previous adhesion site (v), while the newly growing LP actin reaches the next adhesion site and the cycle begins anew (vi). LP ruffling (iib) occurred in the case when the total bond energy connecting LP actin to the edge is greater than the bond energy of nascent adhesion sites to the ECM.

preferential edge attachment of beads to the cytoskeleton (Nishizaka et al., 2000) and strengthen the proposed coupling between actin polymerization and integrin-mediated adhesion (DeMali et al., 2002). As the cell edge extends beyond the contraction-induced attachment sites, the VASP and paxillin aggregates are consolidated. We propose that these adhesion sites will then serve as the anchoring structure for MII force generation in the next contraction.

Upward Bending and the Competition between Ruffling and Periodic Contraction

One of the characteristic features of migrating cells is the formation of ruffles (Felder and Elson, 1990; Totsukawa et al., 2004). Therefore, ruffling reflects an important aspect of motility used by all cells. The upward bending during periodic contractions appears to be driven by the same process as ruffle formation: pulling of LP actin by MII. From a mechanical viewpoint, LP bending and ruffling require roughly similar forces, 150 pN/μm (Abraham et al., 1999; Bohnet et al., 2005; Felder and Elson, 1990). Both periodic contraction and ruffling occur in the LP region, reflect an upward bending force, depend on MII activities (Totsukawa et al., 2004), and can propagate laterally (Döbereiner et al., 2006; Machacek and Danuser, 2006).

In the case of periodic contractions, edge-adhesion strength rises due to concentration of integrin clusters at the front of the LP contractile module. Once adhesion sites are initiated, the weakest link of the FN-integrin-actin connection is the interaction with actin (2 pN) and not the connection with FN (20 pN) (Jiang et al., 2003). In contrast, decreased adhesion strength leads to ruffling. In addition, decreasing MII activity, which reduces adhesion-site formation, also increases ruffling (Machacek and Danuser, 2006; Totsukawa et al., 2004). Thus, when forces are generated on LP actin, there is a competition between breaking nascent adhesion sites, i.e., ruffling, and releasing the LP actin from the adhered edge, i.e., periodic contraction (Figure 7). In all cases there is evidence of contractions that are pulling the LP inward and upward.

MII Forces Separate Lamellipodial Actin from the Edge

While part of the actin network remains attached to the substratum, as seen in DIC and EM, we found that LP actin undergoes a process of regeneration and separation every 25 s. The separation, which allows the cell edge to protrude again, is followed by condensation of the LP actin at the back of the LP contractile module, supporting the idea that LP actin turn over is not restricted to actin depolymerization (Ponti et al., 2004; Watanabe and Mitchison, 2002). The condensation is consistent with the network contraction model (Verkhovsky et al., 1999). These results are contrary to the assumption of many theoretical models of steady-state protrusion in which LP actin continuously pushes against the cell edge (Mogilner, 2006). A similar separation and regeneration are observed in vitro after tearing an actin comet tail from the polymerization machinery at the surface of a bead (Marcy et al., 2004). Based on that study, the force necessary to release all the actin filaments from the polymerization machinery at the cell edge is about 50 pN/μm. This is less than the force needed to bend the LP. Thus, several lines of evidence all indicate that the contractile force pulls and detaches a population

of actin from the front of the LP contractile module and condenses it at the back of the LP contractile module.

The growing LP actin could be connected to the cell edge via the polymerization machinery (Pollard and Borisy, 2003), integrins (DeMali et al., 2002), and the cell membrane (Sheetz, 2001). Laser-trap experiments showed that, during LP-actin pulling, connections are formed with integrins at the very front of the LP contractile module. This led to adhesion-site initiation and immobilization of paxillin and VASP close to the cell edge. However, LP actin is released from the early adhesion sites. The adhesion force between LP actin and the cell membrane, 150 pN/μm, could be estimated from tether experiments (Sheetz, 2001). Hence, the forces generated during LP-actin pulling that are responsible for cell-edge retraction are also sufficient to cause the subsequent release of the network from the polymerization machinery or the cell membrane. That VASP was split between the cell edge and the adhesion sites supports that the rupture is occurring between the polymerization machinery and the LP actin, consistent with the immediate regrowth of a new LP-actin network after separation.

Are Periodic Contractions Triggered by Variations in Polymerization or Contractility?

Different types of periodic movements of the cell edge have been observed in many different cell types (Döbereiner et al., 2006; Dubin-Thaler et al., 2004; Machacek and Danuser, 2006). We have shown that periodic contractions are generated by MII force production. Alternative models for explaining the periodicity are biochemically mediated changes in actin-polymerization rates (Machacek and Danuser, 2006). Indeed, fluorescence-speckle microscopy experiments performed on epithelial cells show oscillations in actin-polymerization kinetics in the LP that correlate with the cell-edge retraction and protrusion rates (Ponti et al., 2004, 2005). We found a linear dependence between LP width and the period of retraction (Giannone et al., 2004), an observation that is consistent with our hypothesis that the rate of LP-actin growth sets the contractile cycle period (Figure 1). In epithelial cells, the slower actin flow (5–8 nm/s) is associated with an increased period between contractions (100 s) (Ponti et al., 2004), suggesting that these oscillations could be related to the periodic regeneration of LP actin we describe in fibroblasts. However, different types of periodic movements exist in epithelial cells, fibroblasts, fly cells, and T cells, suggesting different modes of regulation. In the case of periodic contractions, we have shown that MII-dependent force generation drives contractions and adhesion-site formation.

The Lamellipodium Is a Labile Mechanical Link

What is the direction of force generated on LP actin by MII? In LP-actin filaments, barbed ends are directed toward the cell edge and the clusters of MII confined behind adhesion rows would generate inward forces. What is the mechanical effect of these inward pulling forces? We observed upward bending of the LP contractile module. A simple way for such bending to occur would be a bilayered system, with one layer being pulled relative to the other. Two populations of actin filaments with distinct dynamics were previously observed to colocalize at the migrating edge of epithelial cells (Ponti et al., 2004). We used TIRF and EM microscopy to show that the dense and cohesive LP actin forms a distinct layer that appears to move over the sparser LM. To illustrate how force pulling the LP actin inward could bend the LP contractile module while causing cell-edge retraction, we used two layers of paper stuck together at the tip to mimic the bond between LP and LM actin (Movie S18). We pulled the top layer from the back to mimic MII activity and anchored the back of the bottom layer to the surface in order to mimic anchoring adhesion sites. This setup caused lifting up of the tip in a manner similar to ruffling. However, if we introduce glycerol to mimic labile adhesions at the tip, the pulling forces applied on the top layer lead to upward bending and cell-edge retraction. This simple experiment demonstrates that our proposed organization of the LP contractile module is consistent with its observed motion.

We have discovered the mechanism that coordinates MII activity with adhesion formation and edge retraction. Previous models based on biochemical signaling (Giannone et al., 2004; Gov and Gopinathan, 2006; Wolgemuth, 2005; Yamazaki et al., 2005) could not explain the complex pattern of edge retraction (Figure 3A). Likewise, it was not understood how the timing and location of MII activity related to adhesion-site formation, particularly in light of evidence showing that MII clusters were found well behind newly forming adhesion sites (Gupton and Waterman-Storer, 2006; Ponti et al., 2004). We propose a model in which MII activity and adhesion-site initiation is coordinated by a physical signal. LP actin serves as this physical signal by transmitting forces between the MII and the cell edge. Thus, our work shows that a mechanical mechanism coordinates spatially isolated biochemical processes to shape cell motility.

Mechanics in Motile Functions

There is an increasing body of evidence indicating that mechanical factors play a significant role in cell functions, particularly in cell motility (Giannone and Sheetz, 2006; Vogel and Sheetz, 2006). The present study illustrates how the cell uses macromolecular complexes in which individual biochemical and mechanical components interact in order to achieve higher-level functions. In such complexes, force acts as a signal that is transmitted over distances and performs functions that could not be achieved by long-range biochemical processes.

EXPERIMENTAL PROCEDURES

Cell Culture

Immortalized MEFs (Giannone et al., 2004) were cultured in DMEM (Gibco) with 10% FBS. Transient transfection of plasmids was

performed with Fugene 6 (Roche) following the manufacturer's protocol. Plasmids included EGFP (Clontech, Palo Alto, CA), paxillin-GFP, α-actinin-EGFP (provided by C.A. Otey, University of North Carolina, Chapel Hill, NC), human long MLCK-EGFP (Dulyaninova et al., 2004) (provided by A.R. Bresnick, Albert Einstein College of Medicine, Bronx, NY), paxillin-DsRed (provided by E.E. Marcantonio, College of Physicians and Surgeons, Columbia University, New York, NY), VASP-GFP (Rottner et al., 1999a) (provided by Juergen Wehland, German Research Center for Biotechnology, Braunschweig, Germany.), MLC-EGFP, and MLC-mRFP (provided by M. Tamada, Columbia University, New York, NY).

Generation of siRNA against MIIA

Immortalized MEFs depleted in MIIA and deficient in MIIB were generated using siRNA targeting mouse nonmuscle MIIA in MIIB KO cells as described in Cai et al. (2006).

Materials

High molecular weight fluorescein dextran (2000000 kDa) was purchased from Molecular Probes. Full-length human fibronectin was purchased from Roche. Hexamethyl disilazane (HMDS) and cytochalasin B were purchased from Sigma. Calyculin A, jasplakinolide, and Blebbistatin were purchased from Calbiochem.

Spreading Assays

MEFs spreading essays were performed on 10 μg/ml FN as previously described (Dubin-Thaler et al., 2004). For BBI (50 μM) experiments, BBI was added during the 30 min incubation and remained through the experiment. For CB (250 nM), jasplakinolide (200 nM) and CalA (20 nM), cells were imaged before and after drug perfusion.

TIRF, DIC, and EPI Microscopy

Sequential DIC and TIRF time-lapse micrographs were recorded on an Olympus IX81 TIRF microscope coupled to a Coherent laser with alternate exposure from DIC and TIRF excitation every 2–5 s. Emitted light was captured via a 60×, 1.45 NA oil-immersion objective and a Roper Scientific CoolSNAP fx camera. The same setup was used in EPI experiments with Hg lamp excitation instead of TIRF. For higher spatial resolution in EPI we used a 100×, 1.35 NA, oil-immersion objective. For higher spatial and temporal resolution in DIC we used a 100×, 1.3 NA Plan-Neofluor (Carl Zeiss) objective on an inverted Axiovert 100 TV microscope with an analog video camera, as previously described (Giannone et al., 2004).

Laser-Trap Experiments

Silica beads (0.64 μm, Bangs Laboratories) were coated with diluted FN7-10 trimer, as described previously (Jiang et al., 2003). Briefly, biotinylated ovalbumin beads were coated with avidin neutralite, before being coupled overnight with biotinylated FN trimer diluted with biotinylated BSA. With an optical-gradient laser trap (40 pN/μm), FN-coated beads were held at the cell edge during periodic contractions. In those conditions of single FN trimers binding, one or few FN-integrin-actin connections are formed, being at a suboptimal level of connection with the actin flow. The movement of the bead restrained by the laser trap was recorded until the bead was finally pulled out of the trap.

EM Microscopy

Correlative light EM was performed as described (Svitkina and Borisy, 1998). Briefly, α-actinin-GFP transfected cells were mounted on an Olympus IX81 microscope at room temperature. When a cell generated periodic contractions, we performed detergent extraction for 2 min with 1% Triton X-100 in PEM buffer (100 mM Pipes, pH 6.9, 1 mM $MgCl_2$, and 1 mM EGTA) containing 4% 40,000 MW polyethylene glycol (PEG) (Serva). Extracted cells were then washed in PEM buffer and fixed with 2% glutaraldehyde in 0.1 M sodium cacodylate, pH 7.3. Samples for platinum replica electron microscopy were processed as previously described (Svitkina and Borisy, 1998).

Image Analysis

Kymographs were produced and analyzed using ImageJ software (Wayne Rasband, National Institutes of Health, http://rsb.info.nih.gov/ij/) by taking 1-pixel-wide rectangular regions in the direction of edge movement. Deconvolution of the fluorescent signal was performed using Metamorph to clarify the overlay of DIC and fluorescence images. We verified that, besides reducing the fluorescence background, the fluorescence signal was identical before and after deconvolution. Colocalization analysis between MLC-mRFP and VASP-GFP clusters was performed after fluorescence thresholding and binarization using Metamorph. The percentage of superposition between binarized MLC-mRFP and VASP-GFP clusters gave the percentage of colocalization.

The kymographs were analyzed in two stages. In the first stage, filters were designed to detect the location of the features of interest (FOI). In the second stage, these filters were used to detect the FOIs in adjacent kymographs, to track their location, and to create location and velocity maps. The two FOIs used in this work were the cell edge and the summit of the DIC waves. The required software was implemented in a combination of ImageJ extensions and MATLAB. Filters for the cell edge were constructed by manual calibration. Filters for detecting the DIC waves required a machine-learning method (see Figure S2). That method started with a manual annotation of the wave summit in four to five kymographs from each movie. These kymographs were then used as input to a machine-learning algorithm, which generated a filter that imitates the manual detection. The second stage involved applying the filters to all images in the time-lapse and applying a combination of maxima-finding and smoothing techniques to create continuous maps of the location of the cell edge and the wave summit.

Statistical Analysis

Statistical analyses were performed with a Bonferroni post hoc test. Statistical differences between two conditions were determined using Student's t test. All errors are given as ± 1 standard deviation (SD).

Supplemental Data

Supplemental Data include 4 figures, 22 movies, Supplemental Experimental Procedures, and Supplemental References and can be found with this article online at http://www.cell.com/cgi/content/full/128/3/561/DC1/.

ACKNOWLEDGMENTS

We are very grateful to Anne Bresnick, Jurgen Wehland, Carol Otey, Eugene Marcantonio, and Masako Tamada for providing us with respectively the human long MLCK-EGFP, VASP-GFP, α-actinin-GFP, paxillin-DsRed, and MLC-EGFP/MLC-mRFP constructs. The authors would like to thank Robert Adelstein and Adam Meshel for providing MIIB KO and MIIB control cells. The authors would like to thank Ingrid Spielman for her critical readings of the manuscript. This work was supported by grants from NIH.

Received: March 24, 2006
Revised: August 9, 2006
Accepted: December 26, 2006
Published: February 8, 2007

REFERENCES

Abraham, V.C., Krishnamurthi, V., Taylor, D.L., and Lanni, F. (1999). The actin-based nanomachine at the leading edge of migrating cells. Biophys. J. *77*, 1721–1732.

Bear, J.E., Svitkina, T.M., Krause, M., Schafer, D.A., Loureiro, J.J., Strasser, G.A., Maly, I.V., Chaga, O.Y., Cooper, J.A., Borisy, G.G., et al. (2002). Antagonism between Ena/VASP proteins and actin filament capping regulates fibroblast motility. Cell *109*, 509–521.

Bohnet, S., Ananthakrishnan, R., Mogilner, A., Meister, J.J., and Verkhovsky, A.B. (2005). Weak force stalls protrusion at the leading edge of the lamellipodium. Biophys. J. *90*, 1810–1820.

Cai, Y., Biais, N., Giannone, G., Tanase, M., Jiang, G., Hofman, J.M., Wiggins, C.H., Silberzan, P., Buguin, A., Ladoux, B., et al. (2006). Nonmuscle myosin IIA-dependent force inhibits cell spreading and drives F-actin flow. Biophys. J. *91*, 3907–3920.

Cameron, L.A., Giardini, P.A., Soo, F.S., and Theriot, J.A. (2000). Secrets of actin-based motility revealed by a bacterial pathogen. Nat. Rev. Mol. Cell Biol. *1*, 110–119.

DeMali, K.A., Barlow, C.A., and Burridge, K. (2002). Recruitment of the Arp2/3 complex to vinculin: coupling membrane protrusion to matrix adhesion. J. Cell Biol. *159*, 881–891.

Döbereiner, H.G., Dubin-Thaler, B.J., Hofman, J.M., Xenias, H.S., Sims, T.N., Giannone, G., Dustin, M.L., Wiggins, C.H., and Sheetz, M.P. (2006). Lateral membrane waves constitute a universal dynamic pattern of motile cells. Phys. Rev. Lett. *97*, 038102.

Dubin-Thaler, B.J., Giannone, G., Dobereiner, H.G., and Sheetz, M.P. (2004). Nanometer analysis of cell spreading on matrix-coated surfaces reveals two distinct cell states and STEPs. Biophys. J. *86*, 1794–1806.

Dulyaninova, N.G., Patskovsky, Y.V., and Bresnick, A.R. (2004). The N-terminus of the long MLCK induces a disruption in normal spindle morphology and metaphase arrest. J. Cell Sci. *117*, 1481–1493.

Felder, S., and Elson, E.L. (1990). Mechanics of fibroblast locomotion: quantitative analysis of forces and motions at the leading lamellas of fibroblasts. J. Cell Biol. *111*, 2513–2526.

Fradelizi, J., Noireaux, V., Plastino, J., Menichi, B., Louvard, D., Sykes, C., Golsteyn, R.M., and Friederich, E. (2001). ActA and human zyxin harbour Arp2/3-independent actin-polymerization activity. Nat. Cell Biol. *3*, 699–707.

Galbraith, C.G., Yamada, K.M., and Sheetz, M.P. (2002). The relationship between force and focal complex development. J. Cell Biol. *159*, 695–705.

Giannone, G., Dubin-Thaler, B.J., Dobereiner, H.G., Kieffer, N., Bresnick, A.R., and Sheetz, M.P. (2004). Periodic lamellipodial contractions correlate with rearward actin waves. Cell *116*, 431–443.

Giannone, G., and Sheetz, M.P. (2006). Substrate rigidity and force define form through tyrosine phosphatase and kinase pathways. Trends Cell Biol. *16*, 213–223.

Gov, N.S., and Gopinathan, A. (2006). Dynamics of membranes driven by actin polymerization. Biophys. J. *90*, 454–469.

Gupton, S.L., and Waterman-Storer, C.M. (2006). Spatiotemporal Feedback between actomyosin and focal-adhesion systems optimizes rapid cell migration. Cell *125*, 1361–1374.

Henson, J.H., Svitkina, T.M., Burns, A.R., Hughes, H.E., MacPartland, K.J., Nazarian, R., and Borisy, G.G. (1999). Two components of actin-based retrograde flow in sea urchin coelomocytes. Mol. Biol. Cell *10*, 4075–4090.

Jiang, G., Giannone, G., Critchley, D.R., Fukumoto, E., and Sheetz, M.P. (2003). Two-piconewton slip bond between fibronectin and the cytoskeleton depends on talin. Nature *424*, 334–337.

Jiang, G., Huang, A.H., Cai, Y., Tanase, M., and Sheetz, M.P. (2006). Rigidity sensing at the leading edge through {alpha}v{beta}3 integrins and RPTP{alpha}. Biophys. J. *90*, 1804–1809.

Machacek, M., and Danuser, G. (2006). Morphodynamic profiling of protrusion phenotypes. Biophys. J. *90*, 1439–1452.

Marcy, Y., Prost, J., Carlier, M.F., and Sykes, C. (2004). Forces generated during actin-based propulsion: a direct measurement by micromanipulation. Proc. Natl. Acad. Sci. USA *101*, 5992–5997.

Medeiros, N.A., Burnette, D.T., and Forscher, P. (2006). Myosin II functions in actin-bundle turnover in neuronal growth cones. Nat. Cell Biol. *8*, 215–226.

Mogilner, A. (2006). On the edge: modeling protrusion. Curr. Opin. Cell Biol. *18*, 32–39.

Nishizaka, T., Shi, Q., and Sheetz, M.P. (2000). Position-dependent linkages of fibronectin- integrin-cytoskeleton. Proc. Natl. Acad. Sci. USA *97*, 692–697.

Pantaloni, D., Le Clainche, C., and Carlier, M.F. (2001). Mechanism of actin-based motility. Science *292*, 1502–1506.

Pollard, T.D., and Borisy, G.G. (2003). Cellular motility driven by assembly and disassembly of actin filaments. Cell *112*, 453–465.

Ponti, A., Machacek, M., Gupton, S.L., Waterman-Storer, C.M., and Danuser, G. (2004). Two distinct actin networks drive the protrusion of migrating cells. Science *305*, 1782–1786.

Ponti, A., Matov, A., Adams, M., Gupton, S., Waterman-Storer, C.M., and Danuser, G. (2005). Periodic patterns of actin turnover in lamellipodia and lamellae of migrating epithelial cells analyzed by quantitative Fluorescent Speckle Microscopy. Biophys. J. *89*, 3456–3469.

Rottner, K., Behrendt, B., Small, J.V., and Wehland, J. (1999a). VASP dynamics during lamellipodia protrusion. Nat. Cell Biol. *1*, 321–322.

Rottner, K., Hall, A., and Small, J.V. (1999b). Interplay between Rac and Rho in the control of substrate contact dynamics. Curr. Biol. *9*, 640–648.

Sampath, P., and Pollard, T.D. (1991). Effects of cytochalasin, phalloidin, and pH on the elongation of actin filaments. Biochemistry *30*, 1973–1980.

Schoenwaelder, S.M., and Burridge, K. (1999). Bidirectional signaling between the cytoskeleton and integrins. Curr. Opin. Cell Biol. *11*, 274–286.

Sheetz, M.P. (2001). Cell control by membrane-cytoskeleton adhesion. Nat. Rev. Mol. Cell Biol. *2*, 392–396.

Straight, A.F., Cheung, A., Limouze, J., Chen, I., Westwood, N.J., Sellers, J.R., and Mitchison, T.J. (2003). Dissecting temporal and spatial control of cytokinesis with a myosin II Inhibitor. Science *299*, 1743–1747.

Svitkina, T.M., and Borisy, G.G. (1998). Correlative light and electron microscopy of the cytoskeleton of cultured cells. Methods Enzymol. *298*, 570–592.

Tamada, M., Perez, T.D., Nelson, W.J., and Sheetz, M.P. (2007). Two distinct modes of myosin assembly and dynamics during epithelial wound closure. J. Cell Biol. *176*, 27–33.

Totsukawa, G., Wu, Y., Sasaki, Y., Hartshorne, D.J., Yamakita, Y., Yamashiro, S., and Matsumura, F. (2004). Distinct roles of MLCK and ROCK in the regulation of membrane protrusions and focal adhesion dynamics during cell migration of fibroblasts. J. Cell Biol. *164*, 427–439.

Vallotton, P., Gupton, S.L., Waterman-Storer, C.M., and Danuser, G. (2004). Simultaneous mapping of filamentous actin flow and turnover in migrating cells by quantitative fluorescent speckle microscopy. Proc. Natl. Acad. Sci. USA *101*, 9660–9665.

Verkhovsky, A.B., Svitkina, T.M., and Borisy, G.G. (1999). Network contraction model for cell translocation and retrograde flow. Biochem. Soc. Symp. *65*, 207–222.

Vogel, V., and Sheetz, M. (2006). Local force and geometry sensing regulate cell functions. Nat. Rev. Mol. Cell Biol. *7*, 265–275.

Watanabe, N., and Mitchison, T.J. (2002). Single-molecule speckle analysis of actin filament turnover in lamellipodia. Science *295*, 1083–1086.

Wolgemuth, C.W. (2005). Lamellipodial contractions during crawling and spreading. Biophys. J. *89*, 1643–1649.

Yamazaki, D., Fujiwara, T., Suetsugu, S., and Takenawa, T. (2005). A novel function of WAVE in lamellipodia: WAVE1 is required for stabilization of lamellipodial protrusions during cell spreading. Genes Cells *10*, 381–392.

Zaidel-Bar, R., Ballestrem, C., Kam, Z., and Geiger, B. (2003). Early molecular events in the assembly of matrix adhesions at the leading edge of migrating cells. J. Cell Sci. *116*, 4605–4613.

Zhang, X.F., Schaefer, A.W., Burnette, D.T., Schoonderwoert, V.T., and Forscher, P. (2003). Rho-dependent contractile responses in the neuronal growth cone are independent of classical peripheral retrograde actin flow. Neuron *40*, 931–944.